Spherical wave backscatter from straight cylinders: Thin-wire standard targets

Jinyu Sheng[a)] and Alex E. Hay
Department of Physics, Memorial University of Newfoundland, St. John's, Newfoundland A1B 3X7, Canada

(Received 23 September 1992; accepted for publication 16 March 1993)

Analytical results are obtained for the amplitude of a spherical wave backscattered from a solid cylinder immersed in water. The effects of transducer directivity and transmitted pulse duration are included. Backscatter measurements for comparison with theory are made using straight stainless steel wires ranging from 0.13 to 0.26 mm diameter, and acoustic transceivers operating at 1, 2.25, and 5 MHz. The results are used to evaluate the use of thin wires as standard targets.

PACS numbers: 43.30.Ft, 43.20.Fn, 43.30.Yj

LIST OF SYMBOLS

a	cylinder radius
a_0	transducer radius
c	compression wave phase speed in fluid
f_∞	backscatter form factor
h_n	radius of the nth Fresnel zone
i	$(-1)^{1/2}$
k	compression wave number
n_p	number of Fresnel zones
p	pressure amplitude
q	volume flow per unit length
r	perpendicular distance from the cylinder to the field point
r_0	perpendicular distance from the cylinder to the transducer
r_s	distance from the segment dz to the field point
x	$=ka$
D	transducer directivity
$H_0^{(1)}$	zeroth-order cylindrical Hankel function of the first kind
K_v	proportionality constant, Eq. (29)
K_Γ	proportionality constant, Eq. (31)
L	effective length of the cylinder
S	overall system sensitivity constant
$\bar{V}$	maximum receiver output voltage in a pulse system
α_0	attenuation coefficient in water
β	polar angle with respect to the acoustic axis
β_m	angle corresponding to the first zero of D
β_0	half-power angle of the transducer
ϵ_n	Neumann factor: $\epsilon_0=1$, $\epsilon_{n>0}=2$
η_n	Phase shift of the nth wave
λ	wavelength of sound in fluid
ν	frequency
ρ_0	density of fluid
ρ_0'	density of cylinder
τ	duration of transmitted pulse
$\psi(r_0)$	Eq. (13)
$\Gamma(r_0)$	Eq. (11), also Eq. (20)

INTRODUCTION

Sound scattering by cylinders has importance in a wide range of underwater acoustic applications. Acoustic scattering from a solid cylinder of finite length, however, is a difficult problem to fully describe analytically. The boundary conditions at the scatterer have cylindrical symmetry, but at large distances from the cylinder the scattered field spreads spherically if the cylinder is not infinitely long. The problem is more complicated if the incident wave is spherical rather than plane.

Scattering of a plane wave incident on an infinite cylinder has been investigated extensively.[1–3] Studies of plane-wave scattering from finite-length cylinders have also been made.[4–8] It has been shown[5,7] that the scattering characteristics of the cylinder depend on its length relative to the diameter of the first Fresnel zone. For the case in which the length of the cylinder is much greater than the Fresnel zone diameter, the cylinder is in effect infinitely long. If, on the other hand, the length of the cylinder is much less than the Fresnel zone diameter, the cylinder is effectively very short.

Scattering of a spherical wave incident on an infinite cylinder has been studied by Piquette[9] and lately by Li and Ueda.[10,11] Piquette obtained an approximate solution, valid at long wavelengths, by setting the radial and tangential components of the vector potential in the cylinder to zero. Li and Ueda expressed the scattered pressure as a one-dimensional integral of their solution for an obliquely incident plane wave.[3] The integral could not be solved analytically, and its numerical evaluation presented a number of difficulties.[10]

DiPerna and Stanton[12] recently examined the backscattering of a spherical incident wave by cylinders of varying length. It was found that the scattering characteristics are dominated by Fresnel zone effects and the scattered pressure oscillates with the cylinder length caused by wave

[a)]Now at: Department of Oceanography, Dalhousie University, Halifax, N.S. B3H 4J1, Canada.

 © 1993 Acoustical Society of America

Downloaded 12 Oct 2012 to 129.173.23.114. Redistribution subject to ASA license or copyright; see http://asadl.org/terms

interferences due to phase shifts from contributions along the cylinder axis.[12]

In this paper, scattering of spherical waves by a cylinder is reconsidered by including the transducer directivity effects. By using the concept of volume flow, which was first applied by Skudrzyk[13] in deriving a radiation formula, and later adapted by Stanton[7,8,12] to the scattering problem, an analytic solution is obtained in the form of a one-dimensional integral, which is well-behaved, is readily evaluated numerically, and can be solved analytically in certain limiting cases. The results are primarily based on Sheng's doctoral thesis.[14] Similar solutions have been obtained independently by Gurley and Stanton.[15] The number of Fresnel zones insonified by the incident wave at the cylinder governs the behavior of the solution, in a manner analogous to plane wave scattering by finite-length cylinders.[4,7,12] The solution includes the effects of the transducer directivity and the transmitted pulse length. This permits us to address a practical problem: the use of cylindrical wires as standard targets for calibrating monostatic transceivers. Measurements are made using stainless steel wires and narrow-band transceivers at three different frequencies in the megahertz (MHz) range. The measured backscatter is compared with the size/frequency and range dependencies predicted by theory.

Spheres have been widely used as standard targets for calibration purposes,[16,17] but cylinders have not. Spheres have the advantage that their target strength is independent of orientation. In some applications, however, it can be difficult to suspend a spherical target in the acoustic beam. This may be the case, for example, with narrow beam acoustic sounders operating at MHz frequencies. Then, spheres of sizes such that ka is $O(1)$ are so small that scattering from the supporting structure may not be negligible. [It is desirable that ka be $O(1)$ to avoid resonances in standard target applications, since the positions of the resonances are very sensitive to the elastic properties of the target.] In such cases thin wire targets spanning the entire acoustic beam offer a possible alternative, since the support points for the wire are then well outside the beam. This alternative is explored in this paper.

The paper is organized as follows. Section I presents the theory for backscattering of a spherical wave incident on a cylinder of arbitrary length. Backscattering characteristics of monostatic pulsed systems are investigated, incorporating the effects of the transducer directivity. In Section II a brief description of the laboratory setup is given, followed by Sec. III comparing the analytical results with experimental data. Section IV considers the thin-wire standard targets used to determine the overall sensitivity constants of the transceivers.

I. THEORY

We deal only with the case in which the effective length of the cylinder is much greater than its diameter, so that end effects can be assumed to be small.[7] The geometry of the problem is sketched in Fig. 1.

Consider first a continuous plane wave normally incident on an infinite cylinder. The acoustic axis is orthogonal to the longitudinal axis of the cylinder, taken to coincide with the z axis (Fig. 1). An analytical expression for the backscattered pressure was obtained by Faran[1] and can be written as

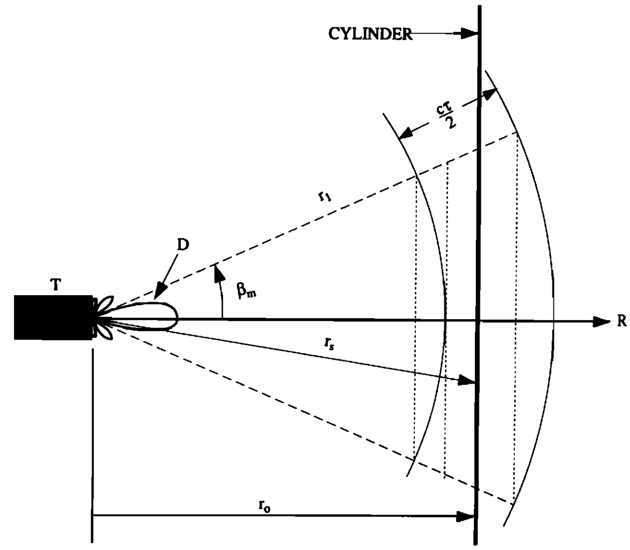

FIG. 1. Coordinate system.

$$p_s=p_i\sqrt{\frac{x}{2kr}}\,f_\infty(x)\exp\left[i\left(kr-\frac{\pi}{4}\right)\right], \tag{1}$$

after suppressing the time dependence. Here, p_i is the incident plane wave amplitude, r is the perpendicular distance from the cylinder to the field point, and $x=ka$, k being the wave number in the ambient fluid and a the radius of the cylinder. In Eq. (1) $f_\infty(x)$ is the far-field backscatter form factor, which can be expressed by

$$f_\infty(x)=-\frac{2i}{\sqrt{\pi x}}\sum_{n=0}^{\infty}(-1)^n\epsilon_n\sin\eta_n\exp(-i\eta_n), \tag{2}$$

where the Neumann factor $\epsilon_n=1$ for $n=0$, and $\epsilon_n=2$ for $n\geqslant1$, and η_n is the phase shift of the nth partial wave.[1]

The far-field backscattered pressure from an infinite cylinder can be analogized by a linear distribution of point sources of constant intensity along the z axis.[7,8] The contribution from an infinitesimal segment of length dz to the total scattered pressure is[7,13]

$$dp_s=-\frac{ik\rho_0'cq}{4\pi r_s}\exp(ikr_s)dz, \tag{3}$$

where c is the sound speed in water, r_s is the distance from the segment dz to the field point, and q is the volume flow per unit length, which is assumed to be invariant regardless of the length of the cylinder. The total pressure is the line integral of dp_s along the axis of the cylinder:

$$\begin{aligned}p_s&=-\frac{ik\rho_0'cq}{4\pi}\int_{-\infty}^{\infty}\frac{\exp(ikr_s)}{r_s}dz\\&=\frac{k\rho_0'cq}{\sqrt{8\pi kr}}\exp\left[i\left(kr-\frac{\pi}{4}\right)\right],\end{aligned} \tag{4}$$

Downloaded 12 Oct 2012 to 129.173.23.114. Redistribution subject to ASA license or copyright; see http://asadl.org/terms

after making use of the result[18]

$$\int_{-\infty}^{\infty} \frac{\exp(ikr_s)}{r_s\,dz} = i\pi H_0^{(1)}(kr),$$

where $H_0^{(1)}$ is the zeroth-order cylindrical Hankel function of the first kind, with asymptotic form

$$H_0^{(1)}(kr) \to \sqrt{2/\pi kr}\,\exp[i(kr-\pi/4)]$$

for large kr.

Comparing Eqs. (1) and (4), the volume flow per unit length of an infinite cylinder can be expressed in the form

$$q = \frac{p_i\sqrt{4\pi x}f_\infty(x)}{k\rho_0' c}. \tag{5}$$

The above expression is also taken to be the volume flow per unit length of a finite cylinder, in accordance with the thin-cylinder assumption made earlier.[7,8,12]

A. Continuous signal

We now consider the case in which the incident wave is spherical and continuous. In the coordinate system shown in Fig. 1, a continuous spherical wave incident on the cylinder can be expressed as

$$p_i = p_* r_* D(\beta)\frac{\exp(-\alpha_0 r_s)}{r_s}\exp[ik(r_s-r_0)], \tag{6}$$

where p_* is the on-axis pressure amplitude at the reference distance r_*, α_0 is the attenuation due to water, D is the transducer directivity, β is the polar angle with respect to the acoustic axis, and r_0 is the perpendicular distance from the cylinder to the transducer. The term $\exp[ik(r_s-r_0)]$ accounts for the phase of the spherical incident wave at different positions along the cylinder.

The volume flow per unit length q in this case can also be expressed by Eq. (5). Based on Eq. (3), the contribution of a segment dz to the total backscattered pressure can therefore be written as

$$dp_s = -ip_i D\frac{\exp(-\alpha_0 r_s)}{r_s}\sqrt{\frac{x}{4\pi}}f_\infty(x)\exp(ikr_s)dz. \tag{7}$$

The total scattered pressure from the cylinder is

$$p_s = -ip_* r_*\sqrt{\frac{x}{4\pi}}f_\infty(x) \times \int_{-L/2}^{L/2} D^2\frac{\exp[ik(2r_s-r_0)-2\alpha_0 r_s]}{r_s^2}dz, \tag{8}$$

where L is now the effective length of the cylinder which, for the geometry in Fig. 1, is determined by the transducer beamwidth. That is,

$$L = 2r_0\tan\beta_m, \tag{9}$$

where β_m is some maximum value of β chosen on the basis of the directivity pattern.

From Fig. 1 we have $r_s = r_0/\cos\beta$ and $dz = r_0/\cos^2\beta\,d\beta$, so that the total backscattered pressure can be written as

$$p_s = p_* r_*\Gamma(r_0)\sqrt{\frac{x}{2kr_0}}f_\infty(x)\frac{\exp(-2\alpha_0 r)}{r_0} \times \exp\left[i\left(kr_0-\frac{\pi}{4}\right)\right], \tag{10}$$

with

$$\Gamma(r_0) = \sqrt{\frac{2kr_0}{\pi}}\exp\left(-i\frac{\pi}{4}\right)\int_0^{\beta_m} D^2\exp[(2ikr_0-2\alpha_0 r_0) \times (\sec\beta-1)]d\beta. \tag{11}$$

It should be noted that in water $\alpha_0 \ll k$ for sounders operating in the MHz range and below, so variations due to $\exp[-2\alpha_0 r_0(\sec\beta-1)]$ in Eq. (11) are small and can be ignored.

The behavior of the above integral depends on the number of Fresnel zones of the cylinder that contribute to the backscattered signal.[12] The radius of the nth Fresnel zone is

$$h_n = \sqrt{nr_0\lambda/2}, \tag{12}$$

where λ is the wavelength of the sound in the ambient fluid. If the main lobe of the transducer beam pattern is spanned by the first Fresnel zone, then the contributions from different positions along the cylinder to the backscattered wave are approximately in phase. This is equivalent to the case of a short cylindrical scatterer. If, on the other hand, the main lobe encompasses many Fresnel zones, then the situation is equivalent to scattering from an infinitely long cylinder.

It is convenient to define the parameter ψ such that

$$\psi(r_0) = \frac{r_0\tan\beta_m}{\sqrt{\frac{1}{2}r_0\lambda}} = \sqrt{\frac{kr_0}{\pi}}\tan\beta_m, \tag{13}$$

which is the ratio of the radius of the main lobe of the transducer directivity pattern, $r_0\tan\beta_m$, to the radius of the first Fresnel zone. Here, $\psi < 1$ corresponds to the short cylinder case. The infinite cylinder case is approached as $\psi \to \infty$. It is more general, therefore, to consider Γ to be a function of ψ. After substituting for kr_0 we have

$$\Gamma(r_0) = \frac{\sqrt{2}\psi(r_0)}{\tan\beta_m}e^{-i(\pi/4)}\int_0^{\beta_m} D^2 \times \exp\left(2i\pi\psi^2(r_0)\frac{(\sec\beta-1)}{\tan^2\beta_m}\right)d\beta. \tag{14}$$

For a circular transducer of radius a_0, uniformly sensitive over its surface, the far-field directivity pattern is given by[19]

$$D = \frac{2J_1(ka_0\sin\beta)}{ka_0\sin\beta}. \tag{15}$$

The half-power angle β_0 is given by

$$ka_0\sin\beta_0 = 1.616. \tag{16}$$

In this paper β_m is defined as the angle corresponding to the first zero of D, or

Downloaded 12 Oct 2012 to 129.173.23.114. Redistribution subject to ASA license or copyright; see http://asadl.org/terms

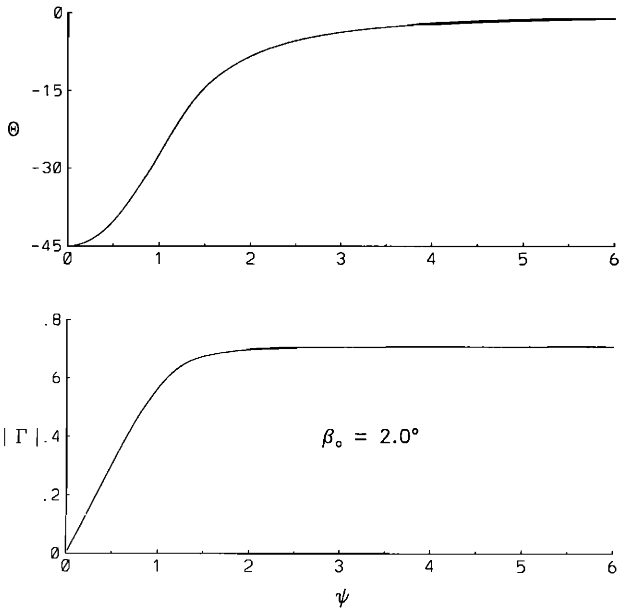

FIG. 2. Calculated values of $|\Gamma|$ and Θ as a function of ψ for a transducer with $\beta_m=4.75°$.

$$ka_0 \sin\beta_m = 3.832, \tag{17}$$

since the region $\beta_0<\beta<\beta_m$ contributes about 25% of the integral, while the contribution from $\beta>\beta_m$ can be ignored.

Writing $\Gamma=|\Gamma|\exp(i\Theta)$, numerical results for $|\Gamma|$ and Θ are shown in Fig. 2 for $\beta_0=2°$ ($\beta_m=4.75°$). Here, $|\Gamma|$ increases linearly for $\psi<0.5$ and tends to 0.7 for very large ψ. Additionally, Θ shifts from $-45°$ at $\psi=0$ to 0° at very large ψ. Analytical results for Γ applicable in the limits $\psi \ll 1$ and $\psi \gg 1$ are (see the Appendix):

$$\Gamma(r_0)=\begin{cases}0.636\psi e^{-i(\pi/4)} & (\psi \ll 1),\\ 1/\sqrt{2} & (\psi \gg 1),\end{cases} \tag{18}$$

consistent with the numerical calculations in Fig. 2. These results imply that the scattered pressure from a short cylinder increases linearly with cylinder length, while the scattered pressure from an infinite cylinder is independent of length, consistent with earlier results[7,8] for plane wave scattering. For example, an expression for the scattered pressure from a short cylinder can be obtained from the infinite cylinder solution by replacing $\Gamma(r_0)$ in Eq. (10) with

$$0.636\sqrt{2}\psi \exp[-i(\pi/4)] = 0.636(L/\sqrt{r_0\lambda}) \times \exp[-i(\pi/4)],$$

from Eq. (18).

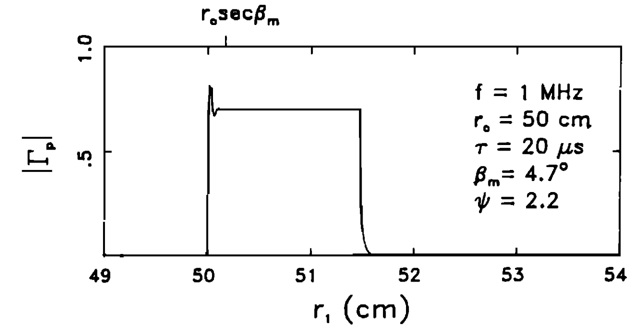

FIG. 3. Variations of $|\Gamma|$ with respect to the position of the pulse front for $\psi=2.2$.

B. Pulsed signal

We next consider the case in which the spherical incident wave is pulsed rather than continuous. Referring to Fig. 1, r_1 is the distance between the transducer and the leading edge of the pulse and τ is the duration of the transmitted pulse. The contribution of a segment dz to the total backscattered pressure takes the same form as that in the continuous incident wave case. The limits of integration for p_s in this case, however, depend on the position of the pulse relative to the axis of the cylinder. By analogy with Eq. (10), we express the total scattered pressure in the form

$$p_s = p_* r_* \Gamma_p(r_0)\sqrt{\frac{x}{2kr_0}} f_\infty(x)\,\frac{\exp(-2\alpha_0 r_0)}{r_0} \times \exp\left[i\left(kr_0-\frac{\pi}{4}\right)\right]. \tag{19}$$

Here, Γ_p is given by

$$\Gamma_p(r_0)=\sqrt{\frac{2kr_0}{\pi}}\,e^{-i(\pi/4)} \times \int_{\beta_1}^{\beta_2} D^2 \exp[2ikr_0(\sec\beta-1)]\,d\beta, \tag{20}$$

where β_1 and β_2 are functions of r_1, namely,

$$\begin{aligned}&\beta_1=0,\quad \beta_2=\arccos(r_0/r_1),\quad r_0\leqslant r_1\leqslant r_0\sec\beta_m,\\ &\beta_1=0,\quad \beta_2=\beta_m,\quad r_0\sec\beta_m\leqslant r_1\leqslant r_0+\tfrac{1}{2}c\tau,\\ &\beta_1=\arccos\left(\frac{r_0}{r_1-\frac{1}{2}c\tau}\right),\quad \beta_2=\beta_m,\quad r_0+\tfrac{1}{2}c\tau\leqslant r_1\leqslant r_0\sec\beta_m+\tfrac{1}{2}c\tau.\end{aligned} \tag{21}$$

Computed values of $|\Gamma_p|$ are plotted as a function of r_1 in Fig. 3 for $\beta_m=4.7°$. The corresponding value of ψ is 2.2. The frequency of the incident wave is 1 MHz, $c=1484$ m/s, $r_0=50$ cm, and $\tau=20\ \mu$s. The half-length of the pulse $\frac{1}{2}c\tau$ is then 1.48 cm, which is much smaller than r_0, as required. These parameter values are typical of the measurements to be presented later.

The results in Fig. 3 indicate a very rapid decrease in

Downloaded 12 Oct 2012 to 129.173.23.114. Redistribution subject to ASA license or copyright; see http://asadl.org/terms

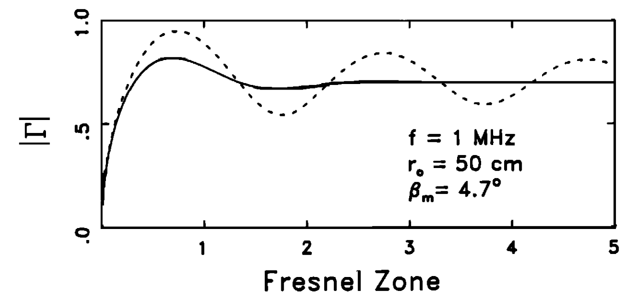

FIG. 4. Variations of $|\Gamma|$ with the number of Fresnel zones for $\psi=2.2$.

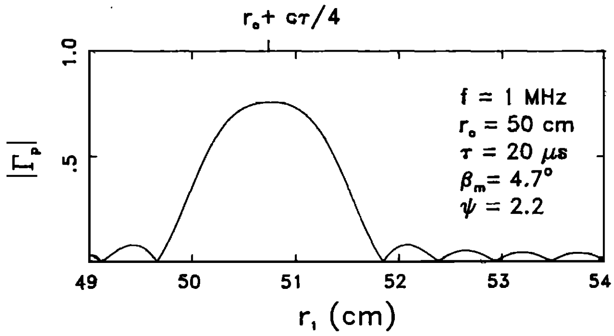

FIG. 5. Same as in Fig. 3, except the data are low-pass filtered (cutoff frequency 75 kHz).

Γ for $r_1 > 51.5$ cm: that is, beyond $r_0+\frac{1}{2}c\tau$. We need therefore consider only the first two of the subintervals listed in (21). From Fig. 1, it can be seen that the effective length of the cylinder L is determined by the leading edge of the pulse in the first subinterval, and by the main lobe of the transducer directivity pattern in the second subinterval. That is,

$$L=\begin{cases} 2\sqrt{r_1^2-r_0^2}, & r_0 \leqslant r_1 \leqslant r_0 \sec\beta_m, \\ 2r_0\tan\beta_m, & r_0\sec\beta_m \leqslant r_1 \leqslant r_0+\frac{1}{2}c\tau. \end{cases} \tag{22}$$

This yields the number of Fresnel zones n_p contributing to the backscatter in the pulsed case:

$$n_p=\begin{cases} (kr_0/\pi)(r_1^2/r_0^2-1), & r_0 \leqslant r_1 \leqslant r_0\sec\beta_m, \\ (kr_0/\pi)\tan^2\beta_m, & r_0\sec\beta_m \leqslant r_1 \leqslant r_0+\frac{1}{2}c\tau, \end{cases} \tag{23}$$

which is obtained by solving for n in Eq. (12) after substituting $L/2$ from Eq. (22) for h_n.

For $\psi=2.2$ (Fig. 3), the main lobe spans several Fresnel zones. As shown in Fig. 4, $|\Gamma|$ increases to a maximum value in the first subinterval $r_0 \leqslant r_1 \leqslant r_0\sec\beta_m$ (50.0 to 50.2 cm), and then oscillates with decreasing amplitude about an intermediate value. In the second subinterval ($50.2 < r_1 < 51.5$ cm), $|\Gamma|$ remains constant. The variations of $|\Gamma|$ in the first subinterval are due to the phase differences introduced as an increasing number of Fresnel zones are insonified.

These variations can be seen more clearly in Fig. 4, which shows the behavior of $|\Gamma|$ as a function of the number of Fresnel zones contributing to the backscatter. The computation was made by setting $\beta_1=0$ and $\beta_2=\arctan(h/r_0)$ in Eq. (20). The solid line in Fig. 4 denotes the results for a directional transducer with $\beta_m=4.7°$, while the dashed line represents the omnidirectional transducer. It can be seen that in both cases $|\Gamma|$ increases with n up to $n\approx 0.7$, at which point a maximum value is reached, the magnitude of which is reduced in the directional case. For $n>0.7$, $|\Gamma|$ oscillates with decreasing amplitude as n increases, although these oscillations are barely discernible for the narrow-beam case. Returning to Fig. 3, n_p increases from 0 to 4.7 as r_1 increases in the first subinterval, and remains constant and equal to 4.7 in the second subinterval. From Fig. 4, the maximum backscattered pressure should occur for $n_p\approx 0.7$, or at $r_1 \approx 50.03$ cm [from Eq. (23)], which is the position of the peak in Fig. 3.

In the measurements to be presented, the backscattered signal was envelope-detected. This involves full-wave rectifying and low-pass filtering the signal. To investigate the effect on the range at which the maximum detected backscatter occurs, a synthetic envelope-detected signal was constructed. The results in Fig. 3 were Fourier transformed, low-pass filtered in the frequency domain, and then inverse Fourier transformed to the time domain. Figure 5 shows the results obtained using a rectangular low-pass filter with a cutoff frequency of 75 kHz, which is representative of the low-pass filter used in the experiments. It can be seen that the maximum signal occurs at $r_1=r_0+\frac{1}{4}c\tau$: that is, when the incident pulse is centered on the cylinder. (The sidelobes in Fig. 5 are due to the filter.)

It is concluded from the above discussion that the maximum backscattered signal, detected in our type of pulsed system, will occur at $r_1\approx r_0+\frac{1}{4}c\tau$, and can be written as

$$p_{\max}=p_* r_* \Gamma \sqrt{\frac{x}{2kr_0}}\, f_\infty(x)\,\frac{\exp(-2\alpha_0 r_0)}{r_0} \times\exp\left[i\left(kr_0-\frac{\pi}{4}\right)\right], \tag{24}$$

where Γ takes the same form as that given by Eq. (14) for the continuous wave case. It can be seen, by comparing Eq. (24) with Eq. (10), that the analytical expression for the maximum scattered pressure in the pulsed case, as considered here using envelope detection, is the same as that for the scattered pressure in a continuous case.

II. EXPERIMENTAL APPARATUS

The experiments were performed in a tank $1.3\times 0.9\times 1.2$ m deep. The water temperature was 23.6 ± 0.3 °C. The acoustic sounders used in the experiments were Mesotech model 810's operating at frequencies of 1, 2.25, and 5 MHz, with a transmitted pulse duration of 20 μs. The receiver circuitry of the Mesotech 810 sounder uses time variable gain (TVG) to compensate for absorption and spreading losses. The absorption coefficient for water was computed using the Fisher and Simmons formula,[20] and the data were recorrected to account for the difference between the actual water temperature in the tank and that for

Downloaded 12 Oct 2012 to 129.173.23.114. Redistribution subject to ASA license or copyright; see http://asadl.org/terms

TABLE I. Radii and values of x ($k_c a$) for the four stainless-steel wires.

a (μm)	x ($k_c a$) ν(MHz)=1.00	2.25	5.00
64	0.27	0.61	1.35
76	0.32	0.73	1.62
102	0.43	0.97	2.15
127	0.54	1.21	2.69

the factory set TVG (10 °C). The received signals are heterodyned down to 455 kHz, and then passed through an envelope detector. The bandwidth of the receiver and envelope detector were about 100 kHz (−3 dB). A multichannel data acquisition system[21] was used to collect the backscatter data from 100 pings. The digitizing rate was 200 kHz. The measured values of $\bar{V}$ represent the 100-ping average of the signal at the range corresponding to the maximum amplitude echo from the wire target.

Stainless-steel surgical wire was used for the cylindrical targets. The wire was attached under tension to a frame 47 cm wide, which could be translated and rotated relative to the acoustic beam. Four different wire radii were used, and are listed in Table I with the corresponding values of $x(ka)$ at the three frequencies. Measurements for each wire were made at seven different distances from the transducer. All wire positions were in the transducer farfield. The transducer beamwidths, wire positions, and corresponding values of ψ are listed in Table II.

III. COMPARISON OF THEORY AND EXPERIMENT

Figure 6 shows a typical example of the backscattered signal at 1 MHz. The width of the backscattered pulse in the figure is determined mainly by the electronic bandwidth. The wire, radius 102 μm, was located 67 cm from the transducer. The value of ψ is about 2.4, so that the main lobe encompasses more than two Fresnel zones. The acoustic data reach a peak value at a range of 67.3 cm. It can be seen that the backscattered voltage profile in Fig. 6 is comparable in shape to the filtered synthetic profile of $|\Gamma|$ in Fig. 5.

The maximum receiver output voltage $\bar{V}$ is related to the maximum backscattered pressure $p_{\max}$ at the transducer through

$$\bar{V}=A[p_{\max}p^*_{\max}]^{1/2}, \tag{25}$$

where A is a proportionality factor and $p^*_{\max}$ is the complex conjugate of $p_{\max}$. From Eq. (24), we have

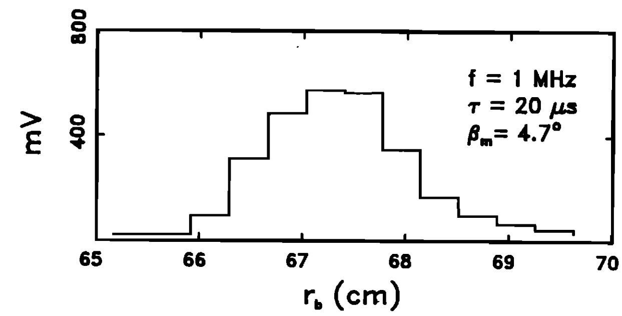

FIG. 6. 100-ping average backscatter profile from a wire located 67 cm from the transducer. The radius of the wire is 102 μm.

$$\bar{V}=S|\Gamma|\frac{\sqrt{x}|f_\infty(x)|}{\sqrt{2kr_0}}\frac{\exp(-\alpha_0 r_0)}{r_0}, \tag{26}$$

where S is an overall system sensitivity constant given by

$$S=Ap_* r_*. \tag{27}$$

After applying the TVG correction, Eq. (26) becomes

$$\bar{V}=S|\Gamma|\frac{\sqrt{x}|f_\infty(x)|}{\sqrt{2kr_0}}. \tag{28}$$

A. Size/frequency variations

We first examine the variation of $\bar{V}$ with cylinder radius and incident wave frequency, at a fixed distance from the transceiver. This permits a direct comparison between measured and theoretical values of the form factor. The term $S|\Gamma|/\sqrt{2kr_0}$ in Eq. (28) is constant. Since x is known, a measured value of $|f_\infty(x)|$ can be determined for each wire from

$$|f_\infty(x)|=K_\nu(r_0)(\bar{V}/\sqrt{x}), \tag{29}$$

where $K_\nu(r_0)$ is a proportionality constant and the subscript ν referring to the frequency. Here, $K_\nu(r_0)$ can be estimated by least squares from measurements made for several different wire radii at fixed r_0 and ν: that is, from the differences between the right-hand side of Eq. (29) and $|f_\infty(x)|$ computed from theory. The resulting estimate of $K_\nu(r_0)$ is used to obtain the measured values of $|f_\infty(x)|$ from $\bar{V}$ through Eq. (29). The results at r_0=85.6 cm are shown in Fig. 7(a). The theoretical values of $|f_\infty(x)|$, denoted by the solid line, were evaluated using Eq. (2) and the physical properties listed in Table III.[22] The measured form factors from all seven positions are shown in Fig. 7(b). The agreement between experiment and theory is quite good: the diffraction extrema in the neighborhood of

TABLE II. Numerical values of ψ for the three frequencies at different ranges.

ν (MHz)	β_0 (degrees)	β_m	$\psi(r_0)$, (r_0 in cm) r_0=38	46	54	62	70	78	86
1.00	2.00	4.75	1.88	2.07	2.24	2.40	2.55	2.70	2.83
2.25	2.05	4.87	2.89	3.18	3.45	3.69	3.93	4.15	4.35
5.00	1.85	4.39	3.89	4.28	4.63	4.97	5.28	5.57	5.85

Downloaded 12 Oct 2012 to 129.173.23.114. Redistribution subject to ASA license or copyright; see http://asadl.org/terms

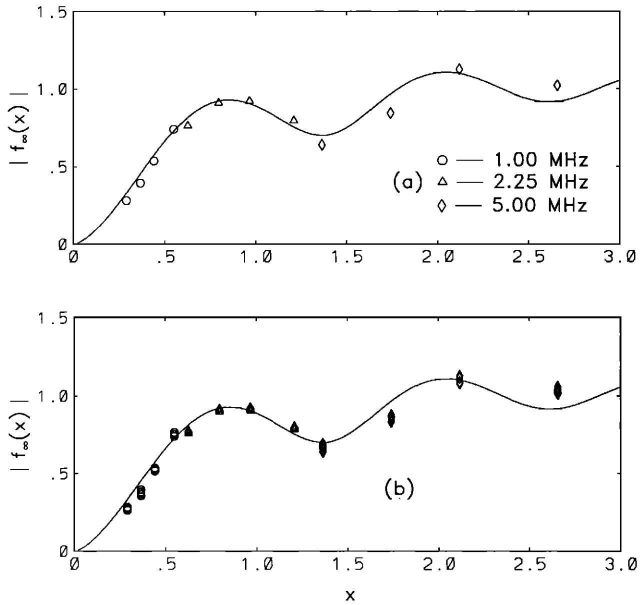

FIG. 7. Comparison between theoretical and measured values of the form factor $|f_\infty(x)|$ at: (a) $r_0 \approx 86$ cm, (b) all seven positions $r_0 \approx 38$, 46, 54, 62, 70, 78, and 86 cm. Theoretical values denoted by solid curve.

$x=1$, 1.5, 2, and 2.5 are reproduced by the measurements, as is the monotonically increasing region at small values of x. The measured values at 5-MHz fit the theory the least well of the three frequencies. There is also more scatter in the 5-MHz data. Both effects are partly attributed to the short wavelength at this frequency, which makes the measurement very sensitive to wire orientation.

The values of $K_v(r_0)$ are listed in Table IV. Also listed are the values of $K_v(r_0)/\sqrt{r}$. These are almost constant, which is to be expected provided $|\Gamma|$ is not strongly dependent on r_0. From Eqs. (28) and (29), we have

$$S=\sqrt{2kr_0}/K_v(r_0)\Gamma, \tag{30}$$

which indicates that the variation of $K_v(r_0)/\sqrt{r_0}$ with respect to r_0 (Table IV) should reflect the variation of $|\Gamma|^{-1}$.

B. Dependence on distance and effective wire length

The dependence of $\bar{V}$ on the effective wire length is described by the function $|\Gamma|$, which in turn depends only on ψ for a given β_m [Eq. (14)]. For a specific transceiver different values of ψ can be realized by changing r_0.

TABLE III. Physical properties of stainless steel and water at 20 °C used in form factor calculation.

Stainless steel[a]		
Density	ρ_0'	7.70×10^3 kg m^{-3}
Compressional wave speed	c'	5762 m s^{-1}
Shear wave speed	c_s'	3185 m s^{-1}
Water		
Density	ρ_0	0.998×10^3 kg m^{-3}
Speed of sound[b]	c	1482 m s^{-1}

[a]See Ref. 22.
[b]The sound speed in the water is calculated using the formula giving by Ref. 19 with zero salinity.

By placing the same wire at different positions, $S\sqrt{x}|f_\infty(x)|$ remains constant, and Eq. (28) can be rewritten in the form

$$|\Gamma|=K_\Gamma(a)\sqrt{2kr_0}\bar{V}, \tag{31}$$

where $K_\Gamma(a)$ is a proportionality constant, representing the factor $[S\sqrt{x}|f_\infty(x)|]^{-1}$. As for K_v, K_Γ is estimated by least squares, minimizing the difference between the right-hand side evaluated from the measurements, and the left-hand side calculated from theory using Eq. (14).

Measured and theoretical values of $|\Gamma|$ are compared in Fig. 8(a), for $a=127\ \mu$m. The measured values of $|\Gamma_m|$ for all four wires are plotted in Fig. 8(b). The solid curve in Fig. 8 represents the theoretical calculation for $\Gamma_m(r_0)$ with $\beta_m=4.75°$ (or $\beta_0=2°$), the values for the 1-MHz sounder. The theoretical curves for the other transceivers are similar. It can be seen from Fig. 8 that agreement between theory and experiment is reasonably good. Also, it can be seen that $|\Gamma|$ is essentially constant over the range of values of ψ covered by the experiment. This explains the earlier observation that the values $K_v/\sqrt{r_0}$ in Table IV are nearly independent of range, and also means that the expression for the scattered pressure tends to that for an infinite cylinder.

IV. THIN-WIRE STANDARD TARGETS

The overall sensitivity constant S for each transceiver can be estimated from the measurements presented in the previous section. From Eq. (28), the least-squares estimate of S is

TABLE IV. The values of $K_v(r)$ and values of $K_v(r)/\sqrt{r}$ at seven different positions for three transducers with frequencies of 1, 2.25, and 5 MHz.

r_0 (cm)	$K_v(r)$ (V^{-1})			$K_v(r)/\sqrt{r}$ ($m^{-1/2}$ V^{-1})		
	ν(MHz)=1.00	2.25	5.00	1.00	2.25	5.00
38	0.669	1.92	7.26	1.09	3.12	11.8
46	0.692	1.97	7.81	1.02	2.91	11.5
54	0.729	2.10	8.46	0.992	2.86	11.5
62	0.753	2.16	8.82	0.956	2.74	11.2
70	0.792	2.26	9.08	0.947	2.70	10.9
78	0.830	2.39	8.48	0.940	2.70	9.62
86	0.877	2.46	9.75	0.946	2.65	10.5

Downloaded 12 Oct 2012 to 129.173.23.114. Redistribution subject to ASA license or copyright; see http://asadl.org/terms

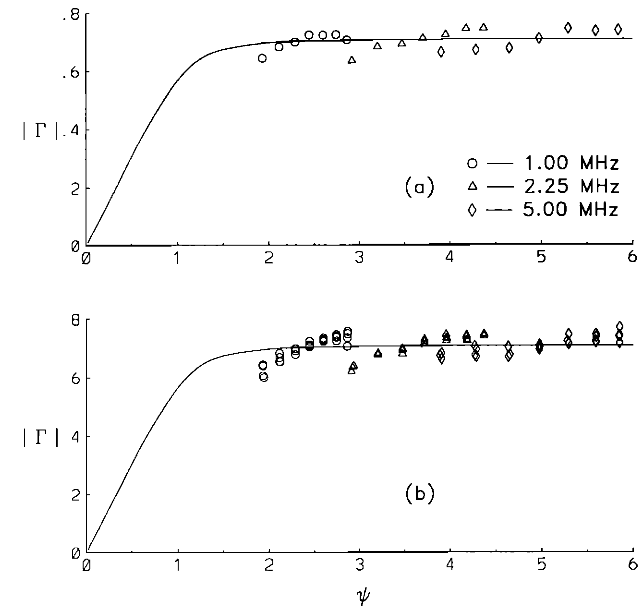

FIG. 8. Comparison between theoretical and measured $|\Gamma|$ for: (a) $a=127$ μm, (b) all four wires with 64, 76, 102, and 127 μm radius. Theoretical values of $|\Gamma|$ denoted by solid curve.

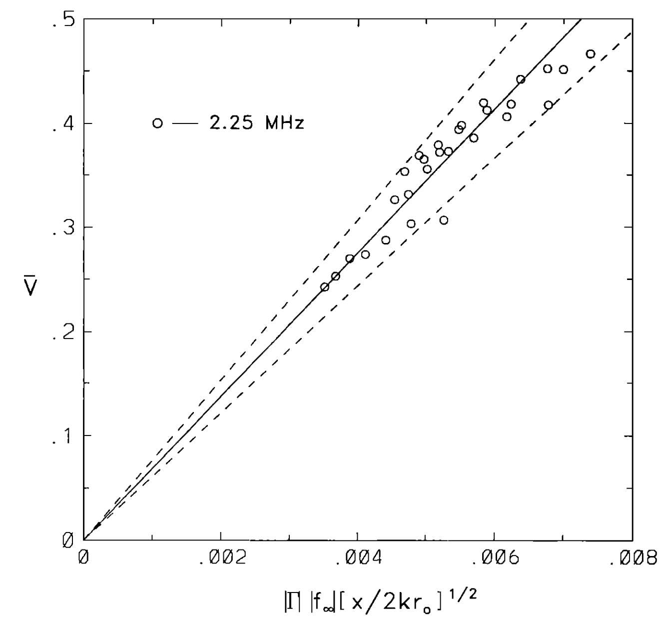

FIG. 9. Plot showing fit of wire measurements to Eq. (28) at 2.25 MHz, using the value of S_w given in Table V (solid line). The dashed lines were used to determine the error bounds listed in Table V for this frequency.

$$S_w=\frac{\Sigma_{j=1}^{7}\Sigma_{i=1}^{4}\left[\bar{V}_{ij}|\Gamma_j|\frac{\sqrt{x_i}|f_\infty(x_i)|}{\sqrt{2kr_j}}\right]}{\Sigma_{j=1}^{7}\Sigma_{i=1}^{4}\left[|\Gamma_j|^2\frac{x_i|f_\infty(x_i)|^2}{2kr_j}\right]},\tag{32}$$

in which the index i refers to the different wire sizes, and the index j to the different positions. The $f_\infty(x_i)$ and Γ_j are computed from theory. The subscript w denotes the wire-determined values of S. The resulting estimates of S_w are listed in Table V. The errors listed in the table are about 15%, and correspond to the full range of the scatter about the best fit, as illustrated by Fig. 9.

These values of S can be compared to estimates of the sensitivities made independently using uniform lead-glass beads suspended in a turbulent jet as standard scatterers.[21] The overall sensitivity determined by backscatter from a cloud of randomly moving particles is[21]

$$S'=B'p_*r_*\left(\frac{3}{16}kc\tau\int_0^{\beta_m}D^4\sin\beta\,d\beta\right)^{1/2}.\tag{33}$$

Using the definition Eq. (27) of S, the above equation can be rewritten in a form more useful for the present purpose:

$$S_g=BS'_g\left(\frac{3}{16}kc\tau\int_0^{\beta_m}D^4\sin\beta\,d\beta\right)^{-1/2},\tag{34}$$

where B is a constant, equal to A/B', and the subscript g indicates values determined from the glass bead experiments. The values of S_g for the three transceivers are listed in Table V, together with the ratio S_w/S_g. The two types of sensitivity estimate agree to within a constant factor, which has a value between 1.3 to 1.4.

The backscatter from fixed wires is coherent, unlike the incoherent scatter from a cloud of particles suspended in turbulence. The wire experiments therefore should represent a measurement of the true peak backscatter amplitude, whereas the glass bead experiments provide an rms amplitude measurement. The more appropriate comparison is therefore with the rms amplitudes of the wire backscatter: that is with $S_w/\sqrt{2}$. As shown in Table V, this accounts for the departure from unity in the values of S_w/S_g.

One can also consider the reciprocal problem: that is, converting the rms backscatter from the suspended particles to equivalent peak backscatter amplitudes. This problem depends on the statistics of the backscattered signals, and has been considered previously[23] for the case of Rayleigh-distributed amplitudes. It was shown that the relationship between the mean and mean square pressure in an envelope detection system is

$$\langle p\rangle^2=\pi\langle p^2\rangle/4.\tag{35}$$

TABLE V. Transceiver sensitivities. S'_g taken from Ref. 21.

ν (MHz)	S_w (V)	S'_g (V)	S_g (V)	S_w/S_g	$S_w/\sqrt{2}S_g$	$S_w/\sqrt{\pi/2}S_g$
1.00	135±22	9.76	98.2	1.37	0.97	1.10
2.25	68.9±7.9	7.68	49.8	1.38	0.98	1.10
5.00	26.0±4.5	4.12	19.8	1.31	0.93	1.05

Downloaded 12 Oct 2012 to 129.173.23.114. Redistribution subject to ASA license or copyright; see http://asadl.org/terms

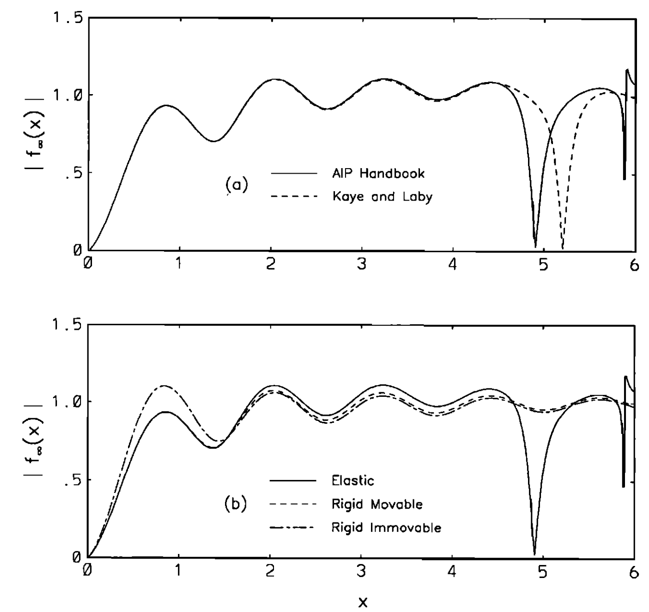

FIG. 10. Theoretical form factor $|f_\infty|$ over the range of $0<x<6$ for the cases of: (a) an elastic cylinder with the physical properties of stainless steel in Table III (a solid line) and the values listed in Ref. 24 (a dashed line); (b) a rigid cylinder with the density of stainless steel and a rigid cylinder of infinite density. The solid line in (b) is same as that in (a).

This factor would increase the values of S_g by $\sqrt{\pi/2} = 1.25$, which would also largely account for the high S_w/S_g ratios in Table V. The fact that this correction does not do as well as the one above is probably due to departures from Rayleigh statistics in the signals backscattered from the jet.

It is useful to consider the possible errors that would be introduced in the overall sensitivity constant S estimates by incorrect material properties used in calculating $|f_\infty|$. Stainless steel is an alloy, and variations in its composition might be important. Theoretical values of the backscatter form factor are shown in Fig. 10 for a number of different cases. Figure 10(a) shows the results for the fully elastic case using the parameters in Table III, and for the values listed in Kaye and Laby:[24] 7.8 g/cm^3, 5980 m/s, and 3297 m/s. For $ka<4$, the differences are small ($<0.3\%$). Large differences occur in the neighborhood of the lowest-order resonance, the oblate-prolate mode, near $ka=5$. Figure 10(b) shows the results for the rigid movable and rigid immovable cases, superposed on the elastic case. (For the rigid movable cylinder, the phase speeds c' and c_s' become infinite. For the rigid immovable cylinder, the density ratio $\rho_0'/\rho_0 \to \infty$ in addition.) These are well known effects in the theory of acoustic resonance scattering:[25] the position of resonances is very sensitive to the elastic properties, particularly the shear wave velocity, whereas beyond the resonances the scatterer behaves as if it were perfectly rigid to a very good approximation. The difference between the rigid and rigid immovable curves in the vicinity of $ka=1$ is due to the displacement of the scatterer about its center of mass, which depends upon the bulk density of the scatterer relative to that of water. We have used two different densities (7.8 and 7.91 g/cm^3) in Fig. 10(a). This density change has little effect on the results near $ka=1$ in Fig. 10(a), and the densities of the different stainless steel alloys are not likely to be much different. The largest value we have found[26] is 8.03 g/cm^3.

The results in Fig. 10 demonstrate that it is unlikely that variations in the material properties of the stainless steel wire targets compared with those assumed in the computations would have contributed significantly to the possible error in the sensitivity constant, because the measurements were made at values of ka less than 3, well below the first resonance. It can also be concluded on the basis of the results in Fig. 10, and the reasonably high tensile strength and corrosion resistance of stainless steel, that this material is well-suited for use as a thin-wire standard target, again provided that resonances are avoided. High tensile strength is required because at MHz frequencies the wire can be no more than a few tenths of a mm in diameter (if ka is to be less than about 3), and the wires must be kept under tension to maintain the aspect of a right circular cylinder. Corrosion resistance is valuable, because the target can remain immersed in water, even seawater, for long periods of time without suffering corrosion damage.

V. CONCLUSIONS

Analytical results have been obtained for the scattered pressure field generated by a spherical wave pulse incident on a cylinder, by using the concept of volume flow as developed by Stanton.[7,8] The effects of the transceiver directivity and the finite duration of the transmitted pulse are included. The solution is conveniently expressed in terms of a single parameter ψ, which is the ratio of the radius of the main lobe of the transducer directivity pattern to the radius of the first Fresnel zone. As would be expected, the behavior of the solution depends on the number of Fresnel zones illuminated by the pulse. It is shown that the solution tends in the appropriate limits to that for very long or very short cylinders. That is, the backscattered pressure is linearly proportional to effective cylinder length for short cylinders, and independent of length for long cylinders.

For typical narrow-beam, narrow-band pulsed transceivers, the expression for the peak detected signal is found to be the same as that for the scattered pressure amplitude in the continuous wave case. It then becomes possible to relate the backscattered pressure from a cylinder of finite length to that for an infinite cylinder. This result is used as the basis for comparing the theoretical expression with measured backscatter amplitudes made using high frequency acoustic transceivers and stainless-steel wire targets. Good agreement is obtained between the measured form factors and those computed from the theory for an infinite elastic cylinder. Good agreement is also obtained between the experimentally and theoretically determined dependence of backscatter amplitude on the range from the transducer. Finally, estimates of the transceiver sensitivities are made from the wire target measurements. These are found to agree well with independent measurements made using backscatter from standard particles in suspension, provided that an appropriate correction is made for

Downloaded 12 Oct 2012 to 129.173.23.114. Redistribution subject to ASA license or copyright; see http://asadl.org/terms

coherent versus incoherent scattering. This result indicates that effective use can be made of thin wires as standard targets in the transducer far field especially at MHz frequencies, for which scattering from the support structure required by other types of fixed target can be problematic.

APPENDIX: Γ IN TWO LIMITING CASES

For simplicity, we consider narrow beamwidths, for which $2i\pi\psi^2(\sec\beta-1)/\tan^2\beta_m$ can be approximated by $i\pi\psi^2\beta^2/\beta_m^2(=ikr\beta^2)$. Therefore Γ in Eq. (14) can be expressed by

$$\Gamma=\frac{\sqrt{2}\psi}{\beta_m}e^{-i(\pi/4)}\int_0^{\beta_m}D^2\exp(i\pi\psi^2\beta^2/\beta_m^2)d\beta. \quad \text{(A1)}$$

For $\psi\ll 1$, the effective length of the cylinder is much smaller than the diameter of the first Fresnel zone. The variations of $\exp(2i\pi\psi^2\beta^2/\beta_m^2)$ in the main lobe of the transducer directivity are small. The integral in Eq. (A1) can then be evaluated by the method of stationary phase, giving

$$\Gamma=\frac{\sqrt{2}\psi}{\beta_m}e^{-i(\pi/4)}\int_0^{\beta_m}D^2\,d\beta \quad (\psi\ll 1). \quad \text{(A2)}$$

The integral $\int_0^{\beta_m}D^2\,d\beta$ in the above expression is constant, and equals $0.450\beta_m$ for narrow beam systems. By using this result in Eq. (A1), then the expression for Γ for $\psi\ll 1$ in Eq. (18) can be obtained.

For $\psi\gg 1$, the effective length of the cylinder is much greater than the diameter of the first Fresnel zone, which is equivalent to very large values of kr for a given β_m. The variation due to $\exp(i\pi\psi^2\beta^2/\beta_m^2)$ in the main lobe is rapid, and its period becomes shorter for larger β. It can be expected that the main contribution to $|\Gamma|$ comes from the first several periods of $\exp(i\pi\psi^2\beta^2/\beta_m^2)$ $[=\exp(ikr\beta^2)]$. We have

$$\begin{aligned}\psi\int_0^{\beta_m}D^2\exp\left(\frac{i\pi\psi^2\beta^2}{\beta_m^2}\right)d\beta &= \psi D_*^2\int_0^{\beta_m}\exp\left(\frac{i\pi\psi^2\beta^2}{\beta_m^2}\right)d\beta\\ &\leqslant \psi\int_0^{\beta_m}\exp\left(\frac{i\pi\psi^2\beta^2}{\beta_m^2}\right)d\beta \quad (\psi\gg 1),\end{aligned} \quad \text{(A3)}$$

where D_* is the value at some β located in the first several cycles of $\exp(i\pi\psi^2\beta^2/\beta_m^2)$. The value of D_* is set to unity in the last expression in Eq. (A3). It can be expected that the inequality in Eq. (A3) becomes an identity when $\psi\to\infty$. Since[27]

$$\lim_{\psi\to\infty}\left[\psi\int_0^{\beta_m}\exp\left(\frac{i\pi\psi^2\beta^2}{\beta_m^2}\right)d\beta\right]=\frac{\beta_m}{2}e^{i(\pi/4)} \quad \text{(A4)}$$

then, the substitution of Eq. (A4) in Eq. (A1) gives the expression for Γ for $\psi\gg 1$ in Eq. (18).

[1] J. J. Faran, Jr., "Sound scattering by solid cylinders and spheres," J. Acoust. Soc. Am. **34**, 405–418 (1951).

[2] L. Flax, V. K. Varadan, and V. V. Varadan, "Scattering of an obliquely incident acoustic wave by an infinite cylinder," J. Acoust. Soc. Am. **68**, 1832–1835 (1980).

[3] T. Li and M. Ueda, "Sound scattering of a plane obliquely incident on a cylinder," J. Acoust. Soc. Am. **86**, 2363–2368 (1989).

[4] W. Williams, N. G. Parke, D. A. Moran, and C. H. Sherman, "Acoustic radiation from a finite cylinder," J. Acoust. Soc. Am. **36**, 2316–2322 (1964).

[5] I. B. Andreeva and V. G. Samovol'kin, "Sound scattering by elastic cylinders of finite length," Sov. Phys. Acoust. **22**, 361–364 (1977).

[6] M. C. Junger, "Scattering by slender bodies of revolution," J. Acoust. Soc. Am. **72**, 1954–1956 (1982).

[7] T. K. Stanton, "Sound scattering by cylinders of finite length. I. fluid cylinders," J. Acoust. Soc. Am. **83**, 55–63 (1988).

[8] T. K. Stanton, "Sound scattering by cylinders of finite length. II. elastic cylinders," J. Acoust. Soc. Am. **83**, 64–67 (1988).

[9] J. C. Piquette, "Spherical wave scattering by an elastic solid cylinder of infinite length," J. Acoust. Soc. Am. **79**, 1248–1259 (1986).

[10] T. Li and M. Ueda, "Sound scattering of a spherical wave incident on a cylinder," J. Acoust. Soc. Am. **87**, 1871–1879 (1990).

[11] T. Li and M. Ueda, "Analysis of echoes from a cylinder that includes the directivity of the transmitter and receiver," J. Acoust. Soc. Am. **87**, 1880–1884 (1990).

[12] D. DiPerna and T. K. Stanton, "Fresnel zone effects in the scattering of sound by cylinders of various lengths," J. Acoust. Soc. Am. **90**, 3348–3355 (1991).

[13] E. Skudrzyk, *The Foundations of Acoustics* (Springer-Verlag, New York, 1971).

[14] J. Sheng, "Remote Determination of Suspended Sediment Size and Concentration by Multi-Frequency Acoustic Backscatter," Ph.D. thesis, Memorial University of Newfoundland (1991).

[15] J. V. Gurley and T. K. Stanton, "Sound scattering by rough elongated elastic objects. III: Experiment," J. Acoust. Soc. Am. **94**, 2746–2755 (1993).

[16] R. H. Wallace, H. V. Hillery, G. R. Barnard, B. M. Marks, and C. M. McKinney, "Experimental investigation of several passive sonar targets," J. Acoust. Soc. Am. **57**, 862–869 (1975).

[17] K. G. Foote, "Optimizing copper spheres for precision calibration of hydroacoustic equipment," J. Acoust. Soc. Am. **71**, 742–747 (1982).

[18] M. Abramowitz and I. A. Stegun, *Handbook of Mathematical Functions* (Natl. Bur. Stand., Applied Mathematical Series, Vol. 55, Government Printing Office, Washington, DC, 1964).

[19] C. S. Clay and H. Medwin, *Acoustical Oceanography: Principles and Applications* (Wiley, New York, 1977).

[20] F. H. Fisher and V. P. Simmons, "Sound absorption in sea water," J. Acoust. Soc. Am. **62**, 558–564 (1977).

[21] A. E. Hay, "Sound scattering from a particle-laden turbulent jet," J. Acoust. Soc. Am. **90**, 2055–2074 (1991).

[22] *American Institute of Physics Handbook* (McGraw-Hill, New York, 1972), 3rd, ed.

[23] A. E. Hay, "On the remote acoustic detection of suspended sediment at long wavelengths," J. Geophys. Res. **88**, 7525–7542 (1983); see also correction, J. Geophys. Res. **90**, 7525–7542 (1985).

[24] G. W. C. Kaye and T. H. Laby, *Tables of Physical and Chemical Constants* (Longmans, London, 1966), 13rd ed., pp. 27 and 29.

[25] L. Flax, G. C. Gaunaurd, and H. Uberall, "The theory of resonance scattering," in *Physical Acoustics XV*, edited by W. P. Mason and R. N. Thurston (Academic, New York, 1981), pp. 191–294.

[26] S. C. Dexter, *Handbook of Oceanographic Engineering Materials* (Krieger, Malabar, FL, 1985).

[27] I. S. Gradshteyn and I. M. Ryzhik, *Table of Integrals, Series, and Products* (Academic, New York, 1980).

Downloaded 12 Oct 2012 to 129.173.23.114. Redistribution subject to ASA license or copyright; see http://asadl.org/terms